Micro and Nano Systems Letters

LETTER

Open Access

Simulation of Germanium-on-Nothing cavity's morphological transformation using deep learning

Jaewoo Jeong[1,2], Taeyeong Kim[1,2] and Jungchul Lee[1,2*]

Abstract

Unique self-assembled germanium structures known as Germanium-on-Nothing (GON), which are fabricated via annealing, have buried multiscale cavities with different morphologies. Due to their unique sub-surface morphologies, GON structures are utilized in various applications including optoelectronics, micro-/nanoelectronics, and precision sensors. Each application requires different cavity shapes, and a simulation tool is able to determine the required annealing duration for a given shape. However, a theoretical simulation inevitably requires simplifications which limit its accuracy. Herein, to resolve such dependence on simplification, we introduce a deep learning-based method for simulating the transformation of sub-surface morhpology of GON over annealing. Namely, a deep learning model is trained to predict GON's morphological transformation from 4 cross-sectional images acquired at different annealing times. Compared to conventional simulation schemes, our proposed deep learning-based simulation method is not only computationally efficient (∼ 10 min) but also physically accurate with its use of empirical data.

Keywords: Deep learning, Germanium-on-nothing, Simulation

Introduction

Compared to the widely used lithography-based manufacturing scheme which only utilizes the surface form factor, the annealing-based silicon-on-nothing (SON) [1] and germanium-on-nothing (GON) [2] fabrication methodology additionally exploits the nanoscale sub-surface components of a semiconductor wafer [3, 4]. By annealing straightly etched hole patterns, micro to nanoscale buried cavities are acquired without a need for a hermetic sealing process. These cavities are formed in various morphologies, from circular pipes to spheres and plates, depending on the shape of initial hole pattern and annealing duration [5]. Such unique product is utilized in applications of diverse domains: photonic crystals [6], pressure sensors [7, 8], microchannels [9], solar cells [2], to name a few.

Each application require different sub-surface morphologies for its appropriate employment. Therefore, as the vertically-etched initial structure transforms into circular pipes, spheres, and finally into plates, annealing must be ceased at the exact moment when a desired cavity morphology is formed. Instead of straightforward optical wave or diffraction-based inspection procedures for surface structures, more elaborate inspection methods are required for these buried cavities. Ultrasonic atomic force microscopy [10, 11], X-ray scanning [12], and optical interferometry [13] are some widely used sub-surface imaging techniques that provide a stack of 2-D profiles. However, these have their own limitations of either low throughput or inoperability under extreme thermal conditions. On the other hand, simulating the transformation of sub-surface morphology would reduce the dependency on these *in-situ* sub-surface imaging

*Correspondence: jungchullee@kaist.ac.kr

[2] Center for Extreme Thermal Physics and Manufacturing, Korea Advanced Institute of Science and Technology, Daejeon, South Korea
Full list of author information is available at the end of the article

process, therefore circumventing their corresponding limitations. While phase field modeling, a specific branch of finite element method (FEM) for solving interfacial problems, is a viable simulation method for GON structures, it inevitably incorporates long computational period (up to 10 h) depending on the mesh size [14, 15]. In addition, phase field modeling is solely based on calculating surface diffusion phenomenon, therefore not taking into account the physical properties of subject material [16], such as crystalline direction.

In this letter, we present a fast (~10 min) deep learning-based simulation methodology of an annealing-based fabrication process from empirical data, namely cross-sectional images of GONs. The images of 4 different annealing duration GON structures are destructively acquired as training data. Then, based on these data at 4 different times, the essential parameters of the cavity shape and morphology's cross-sectional images are simulated throughout these 4 time steps. Our method requires less than 10 min of training and with its use of empirical data in its calculation, all physical properties of the simulation subject have been thoroughly incorporated to the simulation unlike theoretical simulations which require simplifications; for example, phase field modeling solely considers surface diffusion coefficient for simulating the morphological transformation of GON.

Parametrically convolutional Autoencoder (PC-AE)

Figure 1 denotes the overall workflow of the autoencoder-based simulation. Autoencoder is a specific branch of encoder-decoder architectures that solves $F(x)=x$, namely a model that outputs the identical input data. As the name 'encoder-decoder' connotes, encoder component compresses the input data into a smaller size, extracting the input's essential features in doing so. Then, decoder reconstructs the output information in a desired domain, which can be either identical or disparate compared to the input data. For disparate outputs, common applications are scene segmentation [17] and depth map extraction [18], where the output information is utilized. With identical output, on the other hand, either the encoder or decoder is respectively utilized to extract important features from inputs or reconstruct outputs from arbitrarily given features [19]. These encoder-decoder architectures that output the same input are named autoencoders, and this work's autoencoder model utilizes the decoder to reconstruct cross-sectional images from a single arbitrary feature.

While fully convolutional autoencoders are common for image analysis, linear layers are added to this work's model for simulation of not only the cavity images but also the essential parameters depicting the morphology. Therefore, the model is named a 'parametrically convolutional autoencoder' (PC-AE). To train the PC-AE, cross-sectional scanning electron microscopy (SEM) images of GON structures annealed for 5, 15, 60, and 150 min are acquired and binarized. The PC-AE symmetrically consist of 6 layers of convolutional layers and 4 linear layers for both encoder (top row of PC-AE in Fig. 1) and decoder (bottom row of PC-AE, boxed in red). The encoder compresses the image into a single latent variable, which is subsequently reconstructed into 5 parameters using the linear layers of decoder. From these 5 parameters, the original input image is reconstructed using the convolutional layers of decoder. PC-AE's components with orange background is initially trained to output the 5 essential parameters that depict the morphology of input image, denoted as parameter training. Then, while these layers are frozen, the remaining decoder's convolutional layers

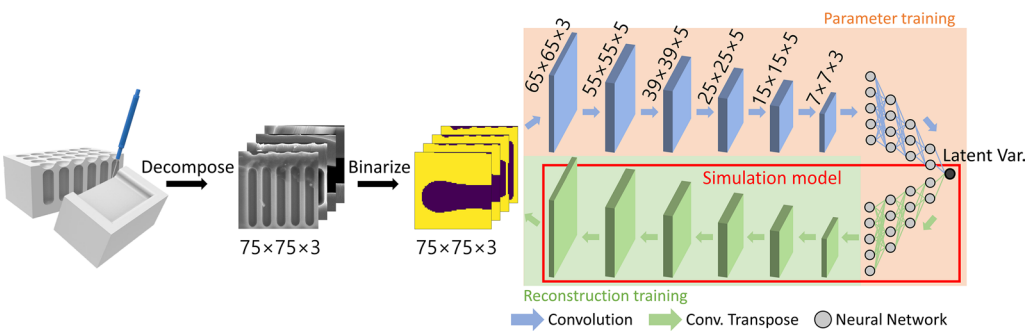

Fig. 1 Pipeline of the deep learning-based sub-surface morphology transformation simulation. The binarized SEM images of GON cross-sections are used as training data, and the deep learning architecture is trained to encode the images into single latent variable and reconstruct it into original images. The pink segment of the entire model is initially trained for parameter training, followed by selective training of green segment for the convolutional reconstruction of original training images

with green background is solely trained to reconstruct the original images from the 5 parameters, named as reconstruction training. After both trainings, the latent variable input for decoder model is iterated to simulate the parameters and sub-surface image. Adam optimizer was used for parameter and reconstruction training with learning rate of 0.001, both aiming to reduce the training loss as mean squared error between labels and reconstructed parameters or images without validation data. A GTX 1660 Super GPU has been used to train the deep learning model with TensorFlow library.

Germanium-on-Nothing fabrication

Vertical and circular holes are patterned via deep reactive ion etching on the surface of a prime-grade Czochralski (100) germanium wafer. The diameter and spacing of the hole patterns are respectively 1.2 μm and 0.8 μm. After removal of organic matters on the surface via diluted ammonia solution ($NH_4OH : H_2O = 1 : 4$ in volume), the wafer is annealed in vacuum (2×10^{-6} Torr) furnace at 890 °C with ramping rate of 25 °C/min. Annealing promotes reduction in surface energy, thereby accelerating the surface diffusion to transform the vertically etched holes.

Figure 2 shows the morphological transformation of GON structures during annealing. At 5 min, the top surface of initial vertical holes is closed to form circular pipes. Then, the membrane walls between the pipes are thinned as the vertical height reduces, forming into sphere-like cavities. Eventually, the individual cavities are merged to form a horizontal plate, and further annealing smoothens the plate's surface roughness. The red alphabets in 5 min image denote the essential parameters that characterize the cavity's morphology: period of hole patterns (P), length of holes (L), spacing between holes (S), diameter of holes (D), and height of roughness (H). Each parameter is normalized by their maxima out of the 4 samples from different annealing durations.

Results and discussion

Figure 3a shows the training result of initial 6500 epochs of parameter training. During the first 500 epochs, training loss (mean squared error) between the label and reconstructed parameter values decreases down to 0.001, which bears about 5 ∼ 10% prediction error. Training loss less than 0.001 is considered valid from empirical inspection, highlighted in blue. As training loss decreases, the R^2 value of the exponential fitting between encoded variables and annealing duration of each variable increases up to maximal value of 0.99956 at epoch 6316. Indeed, as the model learns to reconstruct the essential parameters for each annealing time, it simultaneously learns the temporal correlation incorporated in the input data even without providing any temporal information as training data. The 6500 epochs of training have taken about 10 min, which is a fast computation considering that a FEM-based phase field modeling requires up to several hours depending on the mesh size. Another main advantage of this work's deep learning approach is the use of empirical data. Theoretical simulation such as a FEM-based phase field modeling incorporates simplifications, namely only considering surface diffusion coefficient when modeling the morphological transformation. On the other hand, a deep learning model's use of empirical data automatically incorporates the detailed physical nature such as crystalline direction.

While we have sampled our training data at 4 annealing times to train the model, each at 5, 15, 60, and 150 min, the number of training data required for a successful simulation will depend on the complexity of the phenomenon. The non-linear morphological transformation needs to be characterized by the training data for an accurate simulation after training. For the transformation of GON's subsurface morphology, our training data describes the initial individual cavities

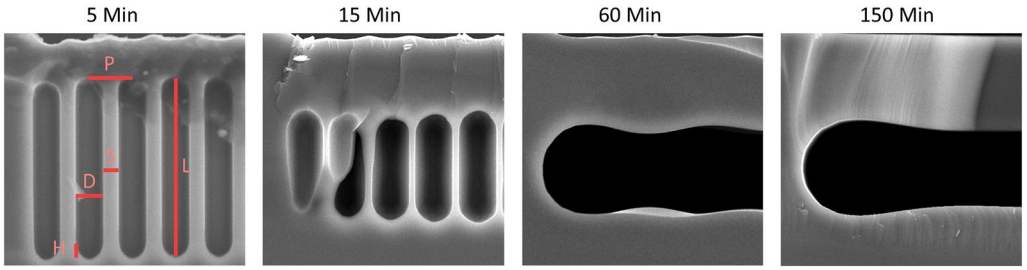

Fig. 2 Cross-sectional SEM images of GON used as training data. Cross-sections are analyzed via destructive test at four different annealing times: 5, 15, 60, and 150 min Red lines on the 5 min image denote the essential parameters extracted from the sub-surface morphology

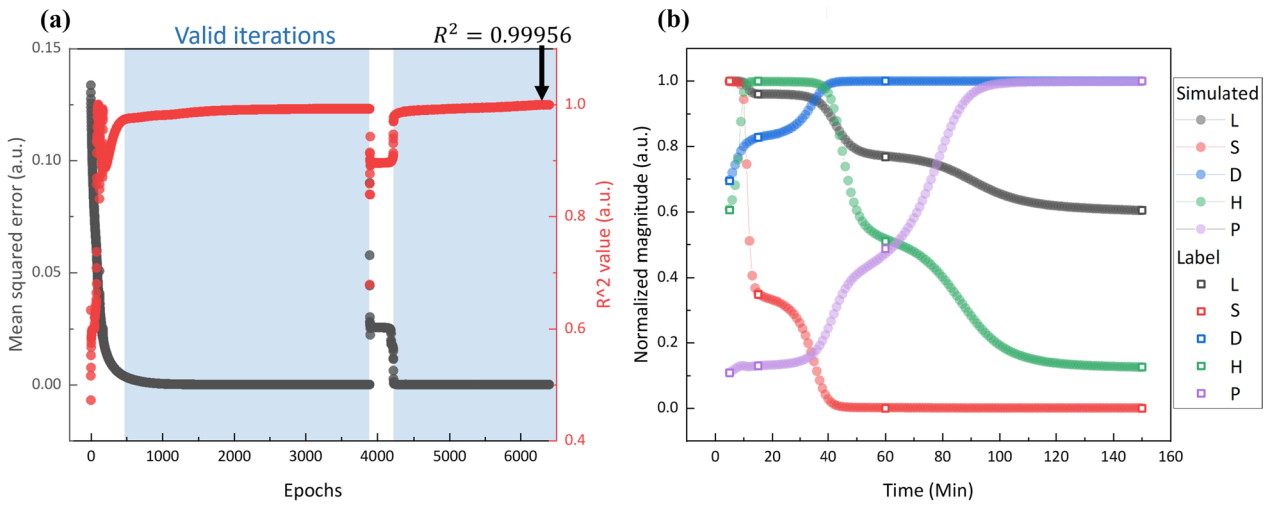

Fig. 3 **a** Parameter training result. As mean squared error decreases, the R^2 value of the fitting between latent variable and annealing time increases. Maximum R^2 value of 0.99956 is acquired at epoch 6318, from which subsequent reconstruction training has been followed. Mean squared error less than 0.005 is considered valid. **b** Simulated parameters after the initial parameter training, with selection of maximum R^2 value. Five parameters are simulated based on the labels at four different times: 5, 15, 60, and 150 min

(5 and 15 min) to a single merged cavity (60 min) and finally the flattened cavity (150 min). Simulation after training is based on these characterization of the essential morphologies during the transformation. For application in a different domain, training data would need to be selected in a similar fashion, with consideration of the morphological complexity and its overall characterization by the training data.

The training iteration with maximal R^2 value was chosen for parameter simulation. While fluctuation of loss value due to the randomness incorporated in deep learning model's optimization process is observed during training around 4000 epochs, the model soon converges to the minimal error, signifying that the model has recovered from the fluctuation and is properly trained. The maximal R^2 is acquired after the fluctuation. Based on the model's competence in understanding the temporal correlation of input images as proven by the high R^2 value, the 5 essential parameters are simulated between 5 and 150 min of annealing as shown in Fig. 3b. One key parameter that is correlated to an insightful observation of GON transformation phenomenon is the spacing (S) between individual cavities. The main determinant to a successful employment of GON structure in varied applications is its appropriate form factor, generally divided as individual or merged cavities. The spacing parameter S precisely describes this disparity. Individual cavities are developed until parameter S reaches zero at 40 min, and a merged plate-like cavity is formed after 40 min. The parametric simulation has specifically characterized the moment when a phenomenon of interest occurs.

Figure 4a shows the subsequent reconstruction training results. The model is trained to reconstruct cross-sectional morphology from the 5 parameters for 1000 epochs, during which mean squared error between label and predicted morphology decreases down to 0.01. Compared to parameter training that was trained for longer epochs, reconstruction training was only proceeded for 1000 epochs to prevent overfitting. A generalized understanding of the training data is crucial to achieving an accurate simulation, and error value of 0.01 has been empirically determined as the appropriate magnitude that simulates the morphological transformation without overfitting. Further training below error value of 0.01 was more prone to constructing physically unnatural morphological transformation. The improvement in quality of model's reconstructions over training is shown in Fig. 4b.

A full simulation after both training stages is shown in Fig. 5. Images at 8 different times are sampled from the exponentially fitted function between the encoded training data and their corresponding annealing time. 4 iterations (a, c, f, and h) are sampled from the region of training data, and the other 4 (b, d, e, and g) are sampled between the training data where morphological transformation could be most adequately portrayed. As shown in the reconstructed images, transformation of both sub-surface cavities and membrane's top surface roughness are accurately simulated. The simulated sub-surface morphologies show a reasonable transformation

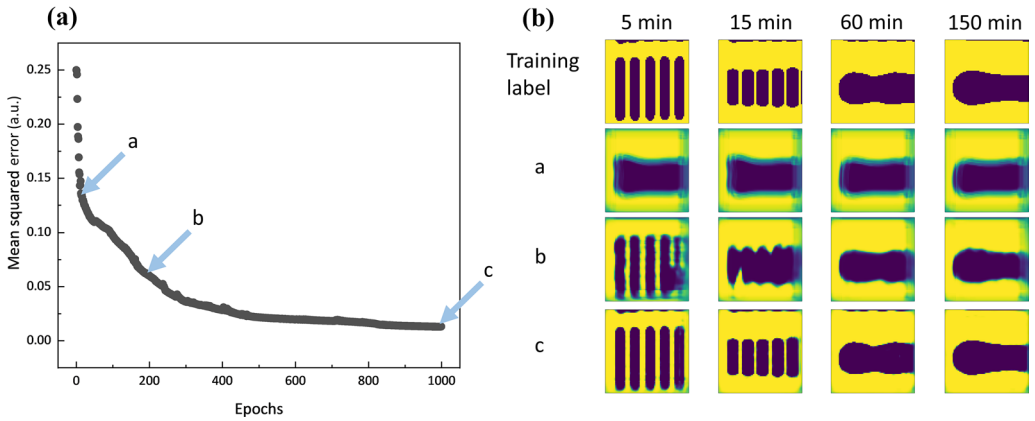

Fig. 4 **a** Reconstruction training result. **b** Comparison of training label reconstructions at three different loss values during training. Training data is accurately reconstructed with longer training

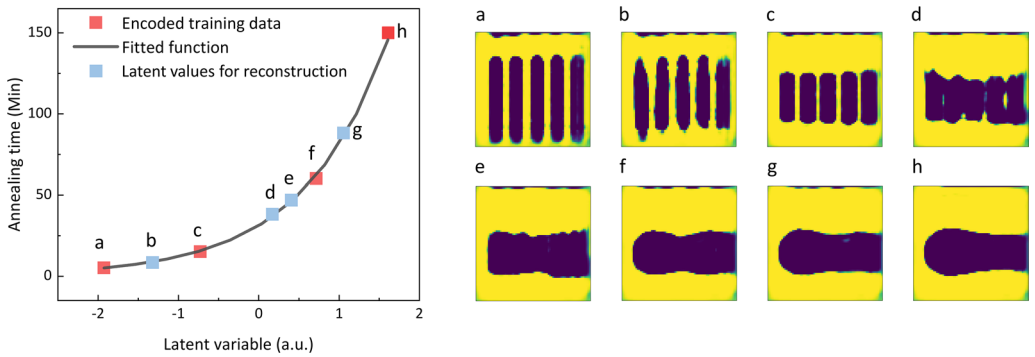

Fig. 5 Simulated sub-surface morphology from the subsequent reconstruction training. Cross-sectional images of sub-surface morphology are simulated based on the same four times: 5, 15, 60, and 150 min, denoted as red boxes (**a**, **c**, **f**, **h**). From their exponential fitting between latent value and annealing time, four latent values denoted by blue squares are for their reconstructions (**b**, **d**, **e**, **g**)

from vertical circular pipes to a merged plate (a-d) and the subsequent flattening process (e-h). Note that iteration 'd' of Fig. 5 is simulated at 40 min when the spacing parameter S reached zero. Indeed, the individual cavities are initiated to merge into a single plate-like cavity. At this point, the sinusoidal roughness of the merged cavity's top and bottom surfaces is analogous to the sinusoidal roughness patterns of individual cavities in iteration C. Further annealing flattens out both top and bottom surfaces of the plate cavity, gradually increasing the period of the sinusoidal pattern. Such increase in period is also depicted by parameter simulation. Magnitude of Fig. 3b's purple line increases with longer annealing time, a trend that the decoder's convolutional layers have learned to reconstruct the 2D morphologies of flattening cavity surfaces. In terms of membrane membrane's top surface, the initially sinusoidal roughness flattens out over annealing, with its increase in sinusoidal period analogous to that of the cavity's surface roughness. Overall, the PC-AE model accurately simulated the surface and sub-surface morphologies as interpreted in this paragraph. Additional file 1: Video S1 contains the resulting simulation by visualizing these reconstructed surfaces in a continuous manner.

Conclusion

In this letter, we present a deep learning-based methodology for simulation of 2D morphological transformation of GON structures during annealing fabrication. 5 parameters that denote GON's sub-surface morphology has been simulated, from which cross-sectional images of morphology has been additional simulated. With deep learning, our empirical data-based simulation incorporates all physical properties related to the phenomenon in a simple fashion, unlike a theoretical simulation which inevitably incorporates simplifications

such as only considering surface diffusion coefficient. The proposed empirical data-based simulation scheme could be widely utilized for various dynamic manufacturing techniques, for example thermal oxidation or etching.

Supplementary Information

The online version contains supplementary material available at https://doi.org/10.1186/s40486-022-00164-5.

Additional file 1: Video S1. Minute-wise simulation of GON's sub-surface morphology transformation.

Acknowledgements
Authors are grateful to the National Research Foundation of Korea for the funds received.

Author contributions
J. Jeong developed the simulation framework and wrote the manuscript. T. Kim fabricated the GON structures. J. Lee supervised the research and the manuscript. All authors read and approved the final manuscript.

Funding
This research was supported by Basic Science Research Program through the National Research Foundation of Korea(NRF) funded by the Ministry of Education (NRF-2020R1A2C3004885 and NRF-2020R1A4A2002728).

Availability of data and materials
The datasets used and/or analysed during the current study are available from the corresponding author upon reasonable request.

Declarations

Ethics approval and consent to participate
The authors declare that they have no competing interests.

Consent for publication
Authors consent the SpringerOpen license agreement to publish the article.

Competing interests
The authors declare that they have no competing interests.

Author details
[1]Department of Mechanical Engineering, Korea Advanced Institute of Science and Technology, Daejeon, South Korea. [2]Center for Extreme Thermal Physics and Manufacturing, Korea Advanced Institute of Science and Technology, Daejeon, South Korea.

Received: 31 October 2022 Accepted: 28 November 2022
Published online: 08 December 2022

References

1. Depauw V, Gordon I, Beaucarne G, Poortmans J, Mertens R, Celis J-P (2009) Proof of concept of an epitaxy-free layer-transfer process for silicon solar cells based on the reorganisation of macropores upon annealing. Mater Sci Eng B 159–160:286–290
2. Park S, Simon J, Schulte KL, Ptak AJ, Wi J-S, Young DL, Oh J (2019) Germanium-on-nothing for epitaxial liftoff of GaAs solar cells. Joule 3(7):1782–1793. https://doi.org/10.1016/j.joule.2019.05.013
3. Sudoh K, Iwasaki H, Hiruta R, Kuribayashi H, Shimizu R (2009) Void shape evolution and formation of silicon-on-nothing structures during hydrogen annealing of hole arrays on si(001). J Appl Phys 105(8):083536. https://doi.org/10.1063/1.3116545
4. Mizushima I, Sato T, Taniguchi S, Tsunashima Y (2000) Empty-space-in-silicon technique for fabricating a silicon-on-nothing structure. Appl Phys Lett 77(20):3290–3292. https://doi.org/10.1063/1.1324987
5. Sato T, Mizushima I, Taniguchi S, Takenaka K, Shimonishi S, Hayashi H, Hatano M, Sugihara K, Tsunashima Y (2004) Fabrication of silicon-on-nothing structure by substrate engineering using the empty-space-in-silicon formation technique. Jpn J Appl Phys 43(1):12–18. https://doi.org/10.1143/jjap.43.12
6. Wong Y-P, Lorenzo S, Miao Y, Bregman J, Solgaard O (2019) Extended design space of silicon-on-nothing MEMS. J. Microelectromechan Syst 28(5):850–858. https://doi.org/10.1109/jmems.2019.2927466
7. Su J, Zhang X, Zhou G, Gu J, Xia C, Zhou Z-F, Huang Q-A (2019) Fabrication of a piezoresistive barometric pressure sensor by a silicon-on-nothing technology. J. Sens. 2019:1–10. https://doi.org/10.1155/2019/5408268
8. Wong YP, Bregman J, Solgaard O (2017) Monolithic silicon-on-nothing photonic crystal pressure sensor. In: 2017 19th International Conference on Solid-State Sensors, Actuators and Microsystems. IEEE
9. Kim J, Song J, Kim K, Kim S, Song J, Kim N, Khan MF, Zhang L, Sader JE, Park K, Kim D, Thundat T, Lee J (2016) Hollow microtube resonators via silicon self-assembly toward subattogram mass sensing applications. Nano Lett 16(3):1537–1545. https://doi.org/10.1021/acs.nanolett.5b03703
10. Sharahi HJ, Shekhawat G, Dravid V, Park S, Egberts P, Kim S (2017) Contrast mechanisms on nanoscale subsurface imaging in ultrasonic AFM: scattering of ultrasonic waves and contact stiffness of the tip-sample. Nanoscale 9(6):2330–2339
11. Ma C, Arnold W (2020) Nanoscale ultrasonic subsurface imaging with atomic force microscopy. J Appl Phys 128(18):180901
12. Servidori M (2007) Determination by high-resolution X-ray diffraction of shape, size and lateral separation of buried empty channels in silicon-on-nothing architectures. J Appl Crystallogr 40(2):338–343
13. Kassamakov I, Grigoras K, Heikkinen V, Hanhijarvi K, Aaltonen J, Franssila S, Haeggstrom E (2013) Nondestructive inspection of buried channels and cavities in silicon. J Microelectromechanical Syst 22(2):438–442. https://doi.org/10.1109/jmems.2012.2227460
14. Kwak T, Kim D (2021) Controlling equilibrium morphologies of bimetallic nanostructures using thermal dewetting via phase-field modeling. Materials 14(21):6697
15. Jeong MG, Kim T, Lee BJ, Lee J (2022) Surrogate model for optimizing annealing duration of self-assembled membrane-cavity structures. Micro and Nano Syst Lett 10(1):1–6
16. Zhang L, Zheng W, Lee J, Wu L, Kim D (2017) A study of morphological evolution of silicon microstructure based on phase field model. Ferroelectrics 520(1):154–158
17. Badrinarayanan V, Kendall A, Cipolla R (2017) Segnet: a deep convolutional encoder-decoder architecture for image segmentation. IEEE Trans Pattern Anal Mach Intell 39(12):2481–2495
18. Yusiong JPT, Naval PC (2019) Asianet: Autoencoders in autoencoder for unsupervised monocular depth estimation. In: 2019 IEEE winter conference on applications of computer vision. pp. 443–451. IEEE
19. Zhao Y, Deng B, Shen C, Liu Y, Lu H, Hua X-S (2017) Spatio-temporal autoencoder for video anomaly detection. In: Proceedings of the 25th ACM international conference on Multimedia. pp. 1933–1941

Publisher's Note